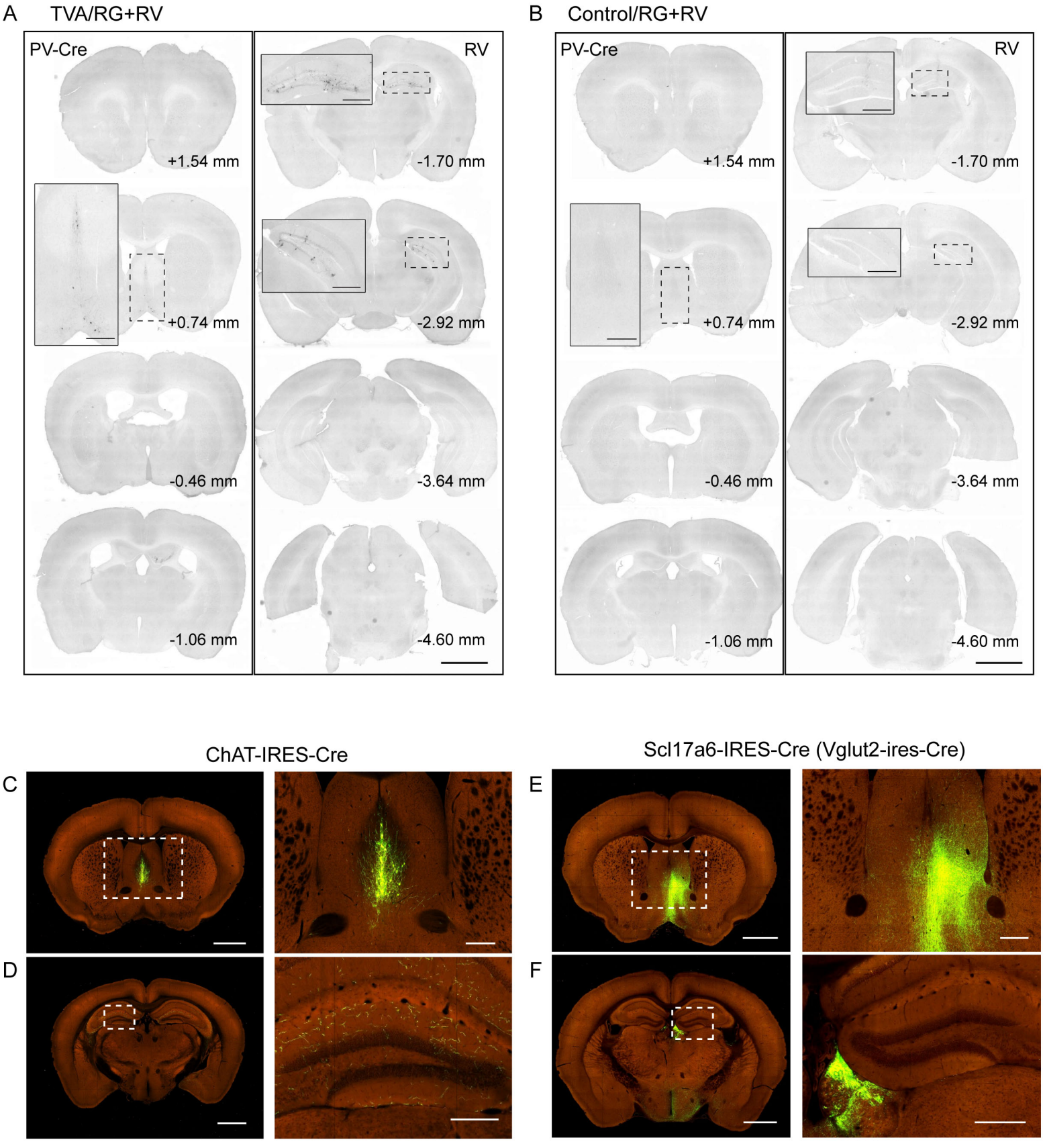

Figure S1 Bao et al., 2017

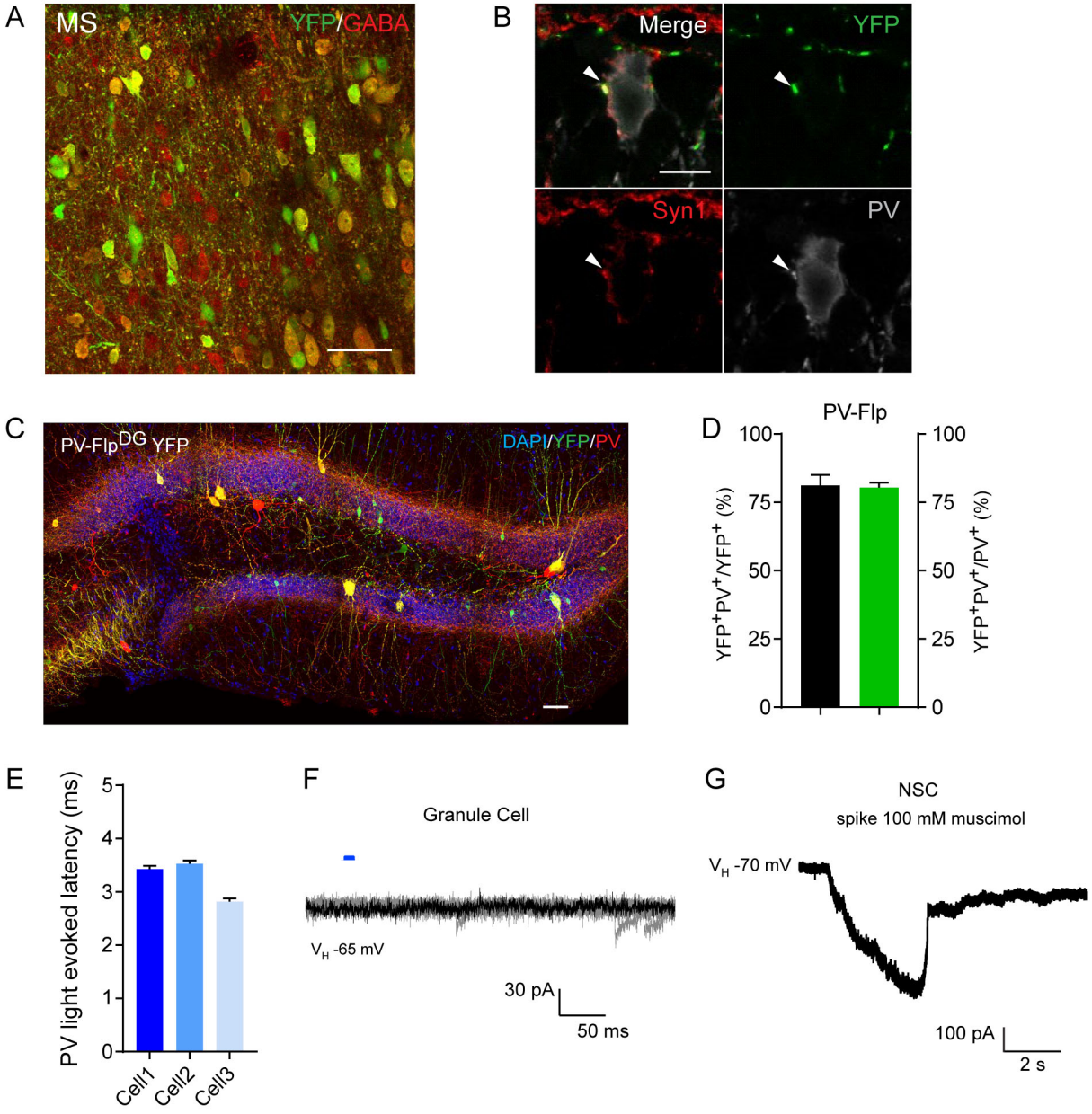

Figure S2 Bao et al., 2017

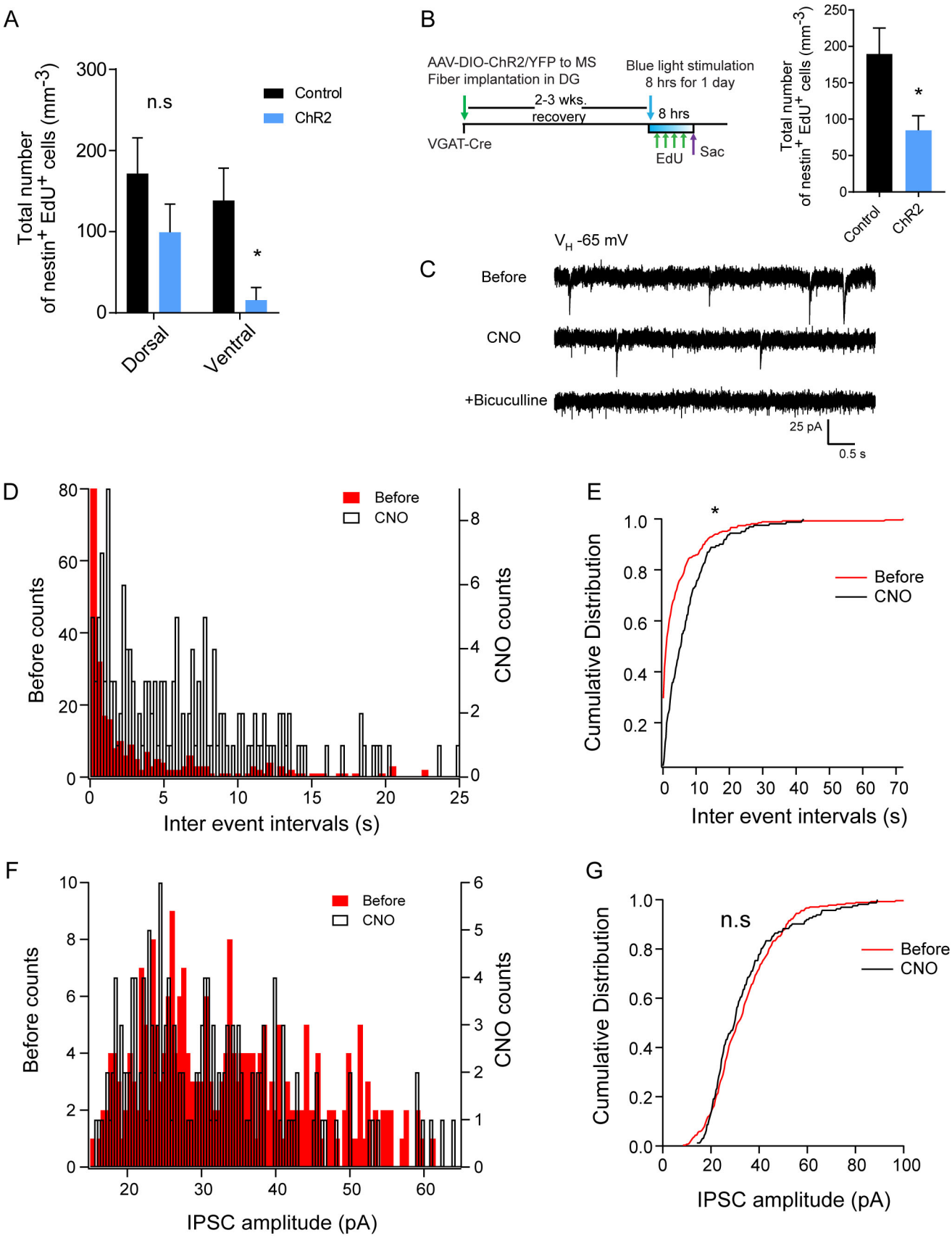

Figure S3 Bao et al., 2017

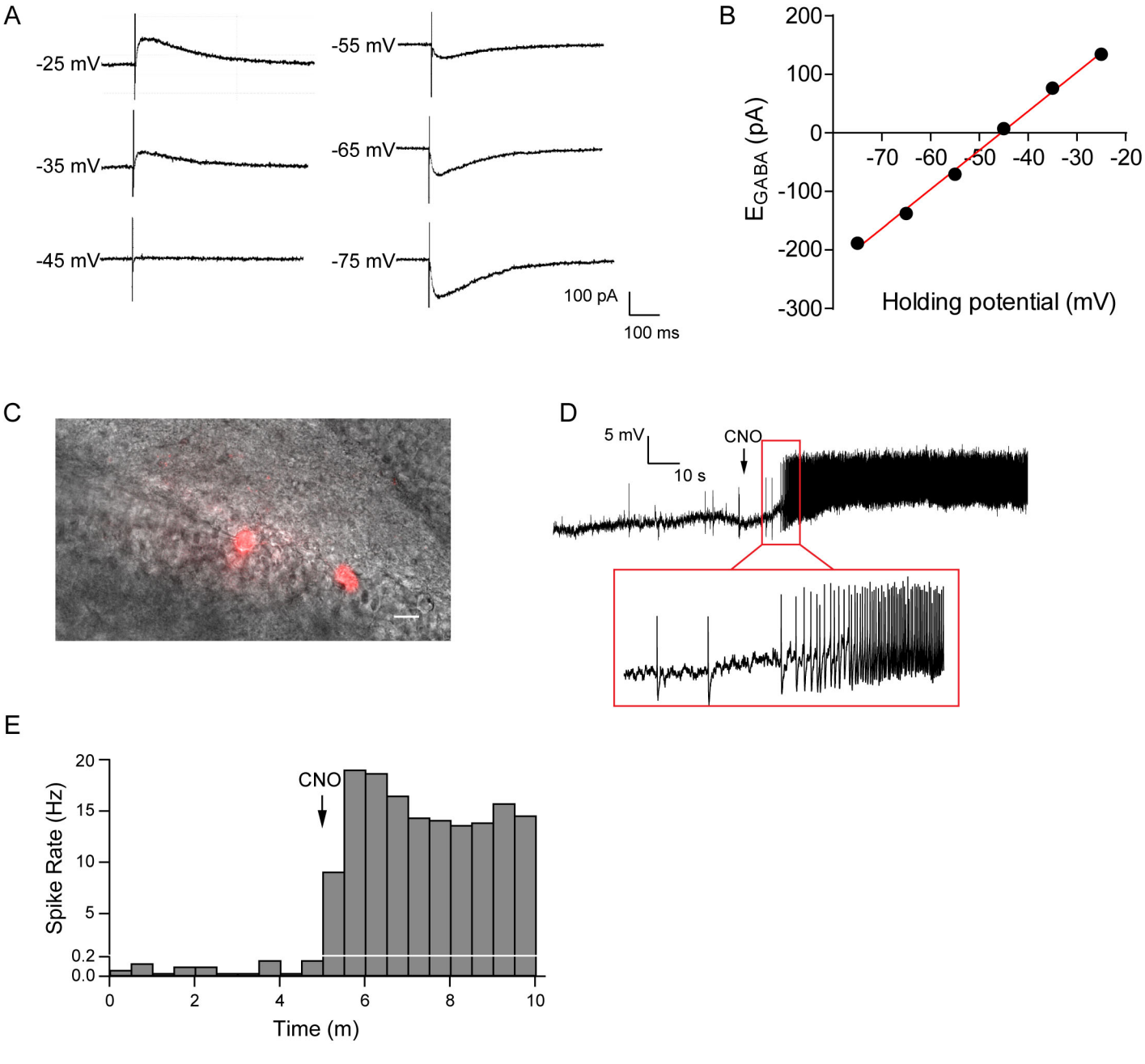

Figure S4 Bao et al., 2017

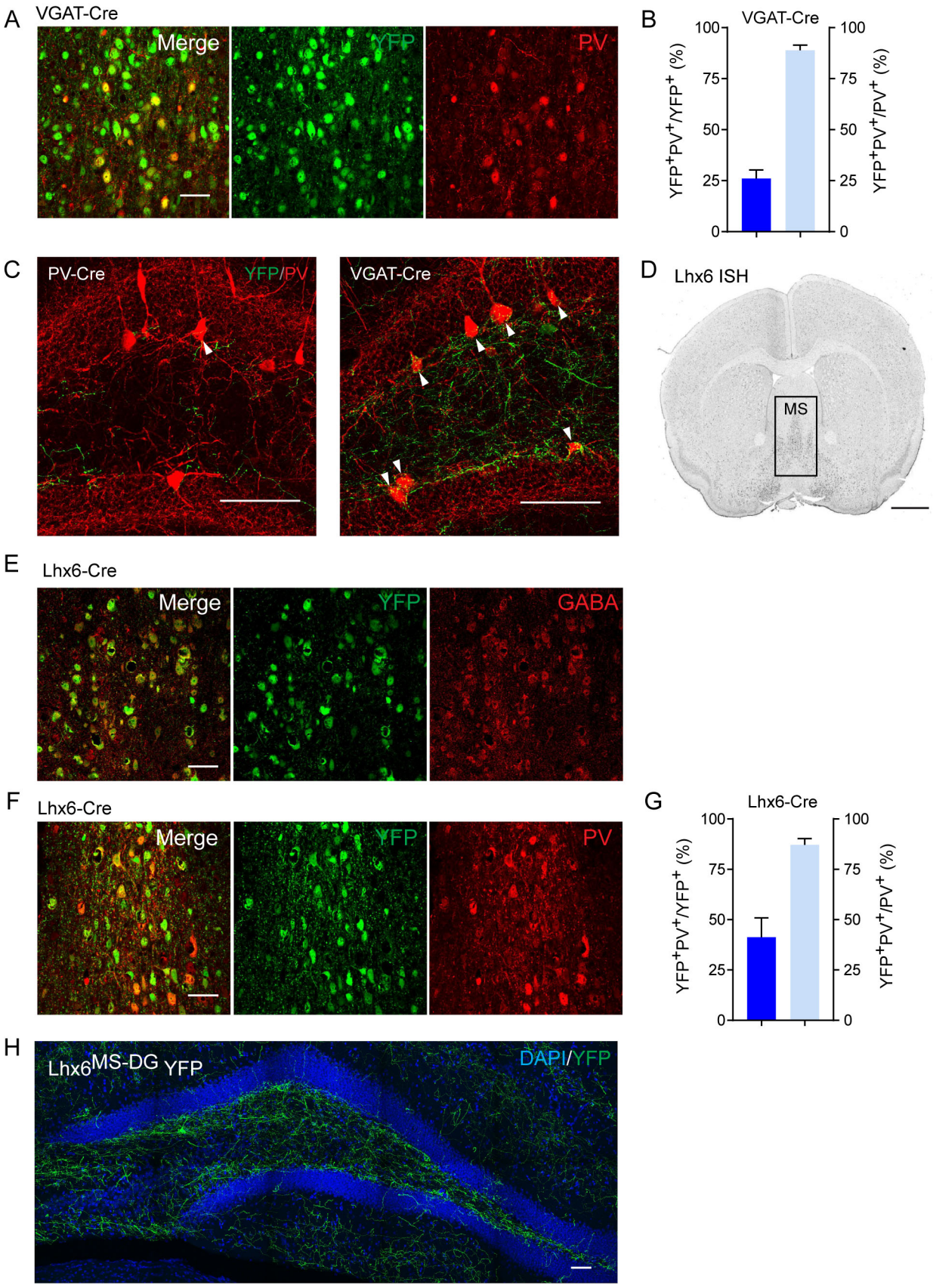

Figure S5 Bao et al., 2017

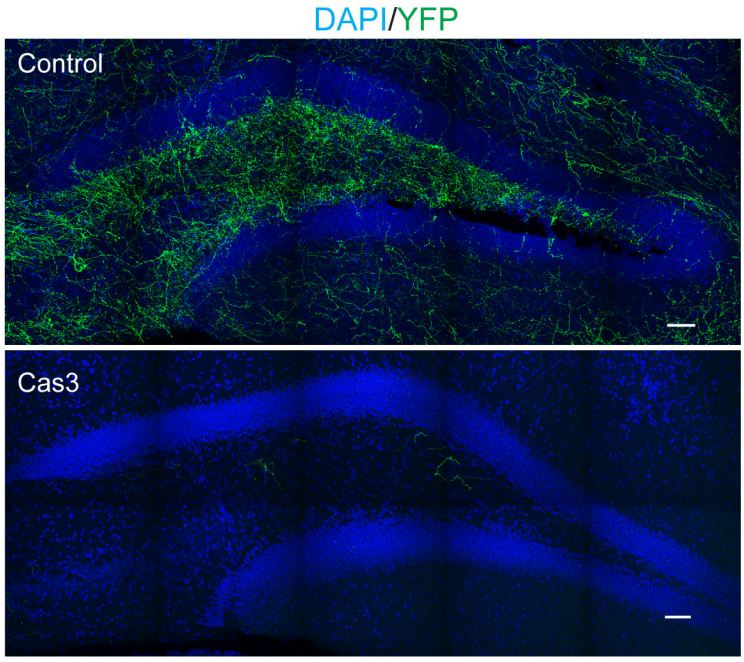

Figure S6 Bao et al., 2017

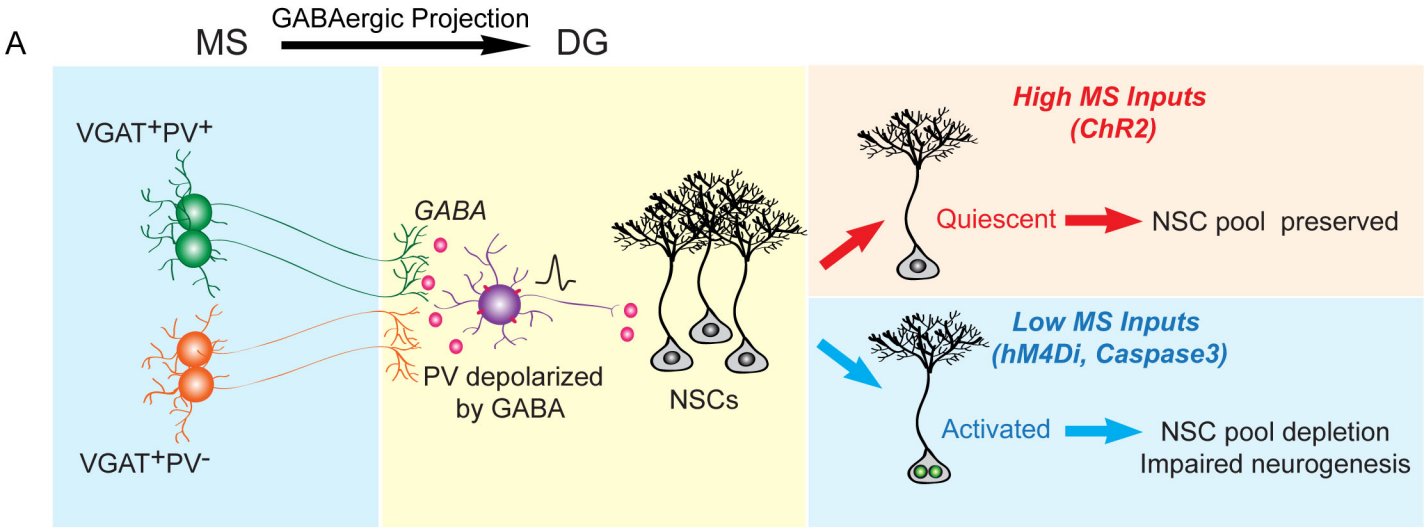

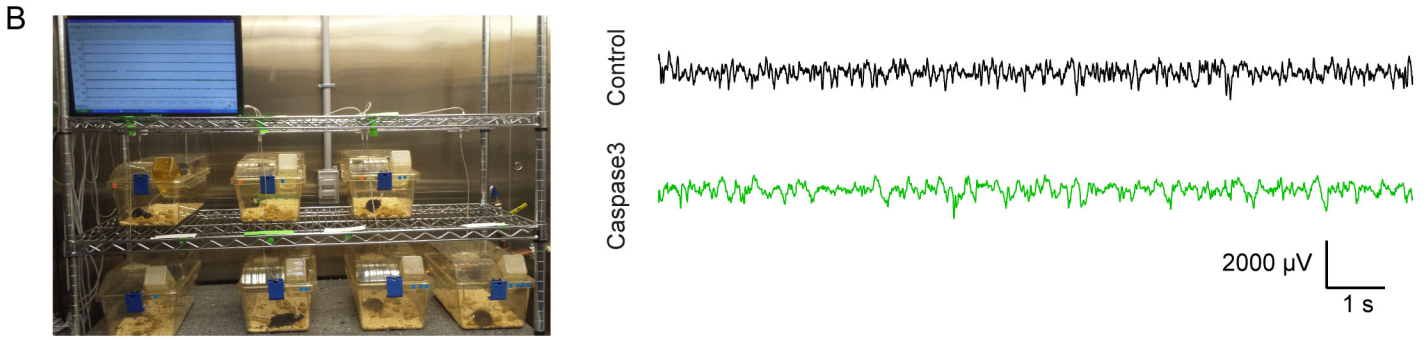

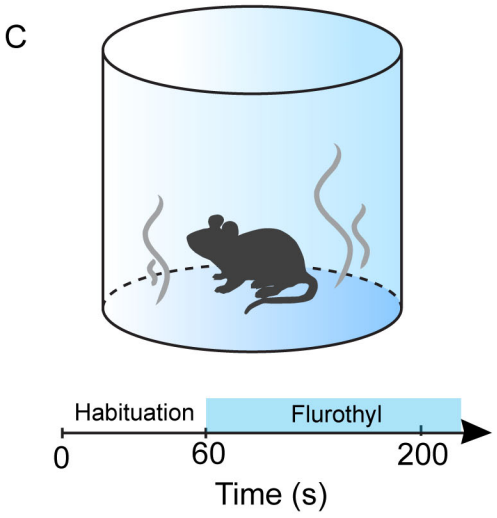

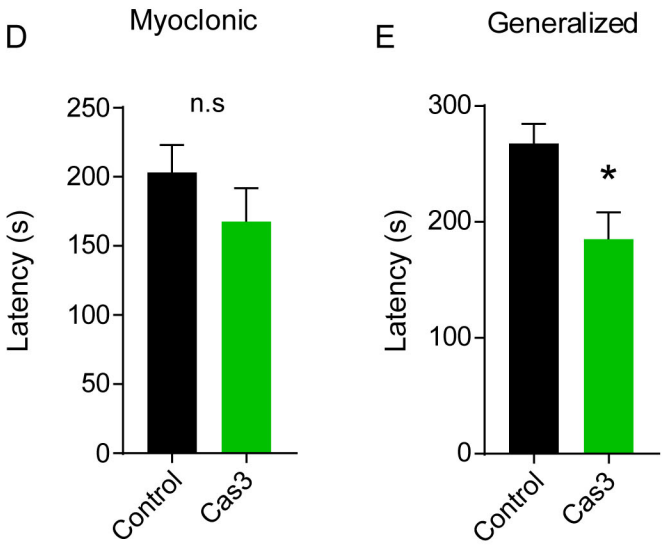

Figure S7 Bao et al., 2017

Supplementary Figure Legends

Figure S1 (related to Fig.1): Additional data on rabies-based tracing and information on anterograde tracing

(A) Specific labeling of the starter PV cells in the dentate gyrus. Distribution of long-distance inputs to the dentate PV interneurons. Rabies-labeled presynaptic input neurons are predominantly located at the MS and the DB. Inputs from other brains are sparse or lacking. Coordinates are based on Bregma. Scale bar: 2 mm (original), 0.5 mm (zoomed in).

(B) No starter PV cells were labeled in the dentate gyrus of the control mice injected with AAV-FLEX-mCherry and AAV-FLEX-RG followed by rabies virus injection. Similar long-distance inputs were lacking in the control mice. Coordinates are based on Bregma. Scale bar: 2 mm (original), 0.5 mm (zoomed in).

(C) Data from C-F were obtained from Allen Brain Atlas Mouse Connectome Project. Scale bar: 1.4 mm for left panels, 0.4 mm for the right panels.

(D) Images of ChAT-Cre mouse injected with flexed rAAV-eGFP in the MS.

(E) Projection sites in the DG of the ChAT-Cre mouse injected with flexed rAAV-eGFP in the MS. Note the lack of axonal collaterals in the neurogenic region.

(F) Images of Scl17a6-Cre (VGLUT2-Cre) mouse injected with flexed rAAV-eGFP in the MS.

(G) Projection sites in the DG of the Scl17a6-Cre (VGLUT2-Cre) mouse injected with flexed rAAV-eGFP in the MS. Note the lack of axonal collaterals in the neurogenic region.

Figure S2 (related to Fig.2): Morphological and functional interaction between VGAT^{MS-DG} projections and quiescent NSCs

(A) Confocal image showing AAV-DIO-YFP specifically labeled GABA^{+} cells in MS of VGAT-Cre mice. Scale bar: 50 μm.

(B) Confocal images showing axonal collaterals from YFP^{+} MS neurons express Synapsin-1 and terminate on the soma of the dentate PV^{+} interneurons. Scale bar: 10 μm.

(C) (D) Characterization of PV-Flp animals. AAV-fDIO-YFP is injected to the DG, and PV antibody is used to characterize the specificity (n=4). Values represent mean ± S.E.M.

Latency of light-evoked PSCs in response to light-pulse stimulation of VGAT^{MS-DG} projections. Cell1, 3.4 ± 0.1 ms, n=4 trials; Cell2, 3.5 ± 0.1 ms, n=15 trials; Cell3, 2.8 ± 0.1 ms, n=12 trials. Values represent mean ± S.E.M.

(E) Overlaid sample traces showing the whole-cell recording (voltage clamp mode) of a dentate granule cell unresponsive to blue light stimulation (light pulse: 470 nm; 10 ms) of VGAT^{MS-DG} projections expressing ChR2. Black line indicates a single example trace.

(F) Sample trace showing radial NSCs are able to respond to $GABA_A$ agonist muscimol following treatment with 200 nM ω-Agatoxin TK.

Figure S3 (related to Fig.3): Validation of the efficiency of inhibitory DREADDs

(A) Comparison of densities of activated radial NSC (nestin$^+$ EdU$^+$) between dorsal and ventral DG blades (n=8 for control, and n=6 for ChR2). *p<0.05 by Student's *t*-test.

(B) Experimental paradigm for 1-d in vivo optogenetic stimulation. Quantification of densities of activated radial NSC (nestin$^+$ EdU$^+$) (n=6 for control and n=5 for ChR2). *p<0.05 by Student's *t*-test. Values represent mean ± S.E.M.

(C) Sample traces showing spontaneous IPSCs (sIPSCs) recorded in a dentate PV$^+$ cell in the absence and presence of CNO for hM4Di inhibition of the $VGAT^{MS\text{-}DG}$ projections (10 μM CNO). sISPCs are blocked by 50 μM bicuculline.

(D) Histogram of spontaneous IPSC inter-event intervals from dentate PV$^+$ cells for 20 minutes before and during CNO application.

(E) Cumulative probability distribution of inter-event intervals from (D). *p<0.05 by Kolmogorov-Smirnov test.

(F) Histogram of the amplitudes of spontaneous IPSCs from dentate PV$^+$ cells for 20 minutes before and during CNO application.

(G) Cumulative distribution of the IPSC amplitudes from (F).

Figure S4 (related to Fig.4): GABA reversal potential in the dentate PV$^+$ interneurons

(A) Sample gramicidin-perforated patch-clamp recording of a dentate PV$^+$ cell in response to electrical stimulation of SGZ/hilus borders where $VGAT^{MS\text{-}DG}$ projections locate.

(B) Quantification of the reversal potential. Red line indicates linear regression, R=0.997.

(C) Sample DIC image of AAV-fDIO-hM3Dq-mCherry labeled DG-PV$^+$ cell for patch recording.

(D) Sample trace showing a DG-PV$^+$ cell responding to CNO application.

(E) Quantification of the spike rate of DG-PV$^+$ cell in the absence and presence of CNO.

Figure S5 (related to Fig.5): Basic characterization of AAV targeting specificity in the MS of the adult PV-Cre and VGAT-Cre mice

(A) Sample confocal images showing YFP labeled MS PV+ cells in VGAT-Cre mice. Scale bar: 50 μm.

(B) Characterization of the percentage of YFP labeled MS PV+ neurons in the VGAT-Cre mice (n=4). Values represent mean ± S.E.M.

(C) Sample confocal images showing the DG-PV$^+$ cells closely associated with MS-DG PV or GABA projections. Arrows indicate the amount of collaterals in DG-PV$^+$ cells associated with MS-DG PV (left) or GABA (right) projections.

(D) In situ hybridization data (ISH) of Lhx6 expression in the MS from Allen Brain Atlas. Scale bar: 1.1 mm.

(E) Sample confocal images showing YFP labeled MS GABA$^+$ cells in Lhx6-Cre mice. Scale bar: 50 μm.

(F) Sample confocal images showing YFP labeled MS PV$^+$ cells in Lhx6-Cre mice. Scale bar: 50 μm.

(G) Summary of the percentage of YFP$^+$PV$^+$ neurons in the MS of the Lhx6-Cre mice (n=3).

(H) Sample confocal image showing AAV-DIO-YFP labeled MS Lhx6$^+$ neurons sending prominent projections to DG. Scale bar: 50 μm.

Figure S6 (related to Fig.6): Reduction of VGAT$^{MS\text{-}DG}$ projections in the caspase mice. Sample confocal images showing significant reduction of VGAT$^{MS\text{-}DG}$ projections in the caspase mice compared to the control mice. Scale bar: 50 μm.

Figure S7 (related to Fig.7): In vivo intra-hippocampal video EEG recording and seizure threshold measurement

(A) A model of a unique GABAergic network for maintaining adult neural stem cell pool and sustainable hippocampal neurogenesis. This unique inhibitory network involves heterogeneous populations of MS GABA neurons and dentate PV$^+$ interneurons with unusual properties, which couples dynamic brain activity to the neurogenic niche to impact quiescence of NSCs, NSC pool maintenance, and hippocampal neurogenesis.

(B) In vivo intra-hippocampal video EEG recording for 48 hours showed no epileptiform activity in either control or caspase VGAT-Cre mice.

(C) Experimental scheme of Flurothyl-induced seizure threshold test in the control and caspase VGAT-Cre mice. Flurothyl administration was terminated upon the occurrence of a generalized seizure.

(D) Quantification of the latency to myoclonic seizure in the control and caspase VGAT-Cre mice. (n=4 for control and n=3 for caspase). Values represent mean ± S.E.M.

(E) Quantification of the latency to generalized seizure in control and caspase VGAT-Cre mice. (n=4 for control and n=3 for caspase). *p<0.05 by Student's *t*-test. Values represent mean ± S.E.M.